Total cross section and resonance spectroscopy for $n+^{124}$Sn

R. F. Carlton
Department of Physics & Astronomy, Middle Tennessee State University, Murfreesboro, Tennessee 37132

J. A. Harvey and N. W. Hill
Oak Ridge National Laboratory, Oak Ridge, Tennessee 37831

(Received 15 May 1996)

The neutron total cross section of ^{124}Sn has been measured over the energy range 0.014–0.315 MeV. An R-matrix analysis has been performed to obtain resonance and average parameters which provide for a complete representation of the neutron entrance channels for the $s_{1/2}$, $p_{1/2}$, and $p_{3/2}$ contributions. The s- and p-wave neutron strength functions have been determined (for a channel radius of 7.23 fm) to be 0.12 ± 0.03 and 1.8 ± 0.2, respectively (in units of 10^{-4}). Limits are placed on the average level spacings and strength functions for the individual partial-wave components. The number of definite $p_{1/2}$ levels exceeds the $p_{3/2}$ levels by the factor 2 and their average strengths differ by the factor 4. s- and p-wave potential scattering radii have been determined to be 6.4 ± 0.2 fm and 10.5 ± 0.3 fm, respectively. Average scattering functions, deduced from the average parameters, have been used to determine the real well depth of an optical-model potential which reproduces these functions. There is evidence of an angular momentum dependence of the real-well potential depth and the level spacings. [S0556-2813(96)02011-0]

PACS number(s): 25.40.Dn, 24.10.Ht, 24.30.Gd, 27.60.+j

I. INTRODUCTION

The even isotopes of tin have zero-spin angular momentum and, because of the magic number of protons and large number of stable isotopes, are useful in exploring nuclear structure. A companion paper [1] has outlined previous investigations of the isotopes of tin that pertain to systematic studies of level structures and properties in both the bound and unbound region. Bound energy levels in these isotopes can be populated *via* stripping and pickup reactions but the resolution afforded by such studies is generally sufficient only to identify levels well below the neutron separation energy. In favorable cases the spin and parity of these levels can be deduced from angular distribution measurements. Neutron transmission studies provide information on unbound levels just above the neutron separation energy. With the high-energy resolution obtainable at the Oak Ridge Electron Linear Accelerator (ORELA) facility, hundreds of levels can be resolved above the separation energy in favorable cases. This provides, for some nuclides, extensive level density information. In addition the determination of spin and parity (J^{π}) of many of the neutron resonances is possible, providing a more microscopic view of their level structures.

Nuclear levels in the unbound region have not been explored extensively for tin. Above 10 keV neutron energy, where other than s-wave interaction is expected, high-resolution neutron total cross-section measurements on zero-spin nuclei can be used to identify the positions and strengths of $1/2^+$, $1/2^-$, and $3/2^-$ levels in this region and provide information for the refinement of model calculations. The tin isotopes are all characterized by low neutron s-wave strength functions since these isotopes lie in the valley between the $3S$ and $4S$ size resonances. Evidence of neutron p-wave interaction was reported in early transmission investigations of the tin isotopes where the maximum neutron energies were from 2 to 10 keV [2]. In the energy range of investigation for the present study, one expects only s- and p-wave interactions to be present due to the relatively high angular momentum barrier for d-wave neutrons and due to the expected low d-wave strength. Thus the parity of all the resonances can be determined through the unambiguous signature of s-wave interactions. Since this work presents the most extensive set of resolved resonances for this isotope, the deduced s- and p-wave strength functions and level spacings will have reduced uncertainty over those previously reported. The spin of the levels can also be deduced in cases where the resonance is sufficiently broad compared to the energy resolution to manifest strong asymmetry or reach the peak cross section. Techniques used in establishing these spins are described in Sec. IV.

Many of the tin isotopes have been the subject of numerous scattering and total cross-section measurements resulting in data covering a broad range of neutron energies (1–24 MeV). These have provided a basis for systematic studies of the optical-model potential and its energy and isotopic dependencies. Wong *et al.* [3] have used potential parameters deduced from simultaneous least-squares fitting of (p,p) and (p,n) scattering on tin isotopes to extract similar parameters for (n,n) scattering on these isotopes at 11 MeV. They find agreement between their predictions and measurements to be comparable to the agreement between those measurements and optimized fits to just the elastic-scattering data [4]. Their optical-model potential parameters are in good agreement with those from the optimization, as well as those of set A of the Ohio University neutron potentials [5]. In addition, optimized fits to inelastic-scattering differential cross sections for the tin isotopes [6] resulted in optical-model parameters in good agreement with these two studies.

In similar studies at lower energies Harper *et al.* have reported on the neutron-excess dependence of the neutron optical potential based upon total cross section [7] and high-precision elastic-scattering [8] measurements. The energy

range covered in these two studies is nearer that of the present investigation, with the scattering at energies, $E_n = 1.00$ and 1.63 MeV, and the total cross sections from 0.3 to 5.0 MeV. The energy dependence of the smoothed average total cross sections was reproduced within 5%, for five of the even-A tin isotopes, using optical-model parameters deduced from fitting of the scattering data and incorporating a standard energy dependence.

Other studies [9,10] in the energy region below 1.5 MeV have sought to exploit the peak in the p-wave neutron strength function for this mass region and the minimum in the s- and d-wave neutron strength functions. They have determined the neutron and radiative strength functions and the potential scattering radii for s-, p-, and d-wave neutrons through fitting of averaged radiative capture and total and differential cross sections. These studies deduced parameters of the optical-model potential in this mass region.

None of these experiments provide for the direct measurement of individual partial-wave contributions. Even the low-energy studies do not have an energy resolution or extend sufficiently low in energy to obtain resolved resonance data and thus spin-and-parity specific information comparable to that of the present study. In those studies any resonance structure has been averaged over and thus include the summed effect of all partial waves contributing to the cross sections. In the present study, the energy and resolution are such that individual resonance parameters are obtained and, more significantly, J^π assignments have made possible the determination of the average neutron properties of ^{124}Sn for s- and p-wave interactions. Thus while other studies have been able to predict strength functions and potential scattering radii from optical potentials deduced from average cross-section data, we have used resolved-resonance data to extract spin-separated strength functions and potential scattering radii, which we have then used to deduce optical-potential parameters required to reproduce these properties. We are then able to determine whether different optical potentials are required to represent the properties corresponding to different parities.

We discuss the experimental details of the measurement in Sec. II. In Sec. III we give the experimental results and in Sec. IV the details of the connection between the R-matrix parametrization and the experiment. We also discuss the bases of the resonance spin and parity assignments. Section V presents the resonance and nonresonant average properties deduced. Section VI presents the results of comparison of the deduced average scattering functions with predictions of a spherical optical-model potential (OMP). Finally we discuss the OMP results in the context of other studies in Sec. VII and the paper concludes with Sec. VIII.

II. EXPERIMENTAL MEASUREMENTS

We have performed transmission measurements by the time-of-flight technique, using neutron pulses from the Oak Ridge Electron Linear Accelerator, at a flight path of 80.300 m for a target of ^{124}Sn. The 140-MeV electron beam burst width was 7.0 nsec and the accelerator was pulsed at 800 bursts per sec at a power level of approximately 7 kW. The resulting neutron burst has a continuous energy spectrum produced by the photoneutron process in tantalum with subsequent moderation in the 15-cm-diam, beryllium-clad, water-filled target housing. Collimators (1.43 cm in diameter) were used both before and after the target to select neutrons from the water-moderated region of the target. The neutron energy resolution function is expected to be a combination in quadrature of the fluctuations in flight-path length and the burst width and has been found to have an approximately Gaussian shape with a full width at half maximum, dE, given by

$$(dE/E)^2 = (1+6E)\times 10^{-6},$$

with E expressed in MeV. Overlap neutrons were eliminated by a 1-g/cm^2 ^{10}B filter and gamma rays were reduced by a 0.73 cm-thick ^{238}U filter and a 0.64-cm-thick Pb filter, placed 5 m from the neutron source.

TABLE I. Isotopic enrichment of the ^{124}Sn sample. Thickness $=0.113$ atoms/b.

Isotope	% present
112	<0.29
114	<0.25
115	0.21
116	3.89
117	2.14
118	6.44
119	2.44
120	9.03
122	1.84
124	73.47

The 45.625-g sample of ^{124}Sn was 1.59 cm in diameter, corresponding to a thickness of 8.82 b/atom. Table I gives the sample enrichment and thickness. The samples were positioned 9 m from the neutron target where the neutron beam was collimated to a diameter of 1.4 cm. The samples were cycled into and out of the neutron beam under computer control with a cycle time of approximately 10 min per sample. A 10-min run per cycle was also made with no sample in the beam. We used a neutron monitor to compensate for fluctuations in the neutron production rate during the three day interval and a total of 39 h of data collection. The three individual runs were each corrected for deadtime and then added to form the final data set.

Neutrons were detected by an NE110 proton recoil detector 7.6 cm in diameter and nominally 2 cm thick. The plastic scintillator was optically coupled to an RCA 8854 photomultiplier tube which was operated in a ''selective gating'' mode. In this mode, four energy windows are established, corresponding to neutron crossover energies of 220, 650, and 2000 keV. Logic for gating event deadtime in the time digitizer is then determined as follows: (a) a single stop per start if an event was identified in time as a gamma flash and occurred in windows 1, 2, or 3 or (b) an event occurred in window 4 at any time. For all other events, the system operated in a multistop per start mode with an 1104 nsec deadtime for signal processing. Additional details concerning the data acquisition have been reported in detail elsewhere [11]. These separate pulse height spectra facilitated the determination of the backgrounds and the optimization of the signal-

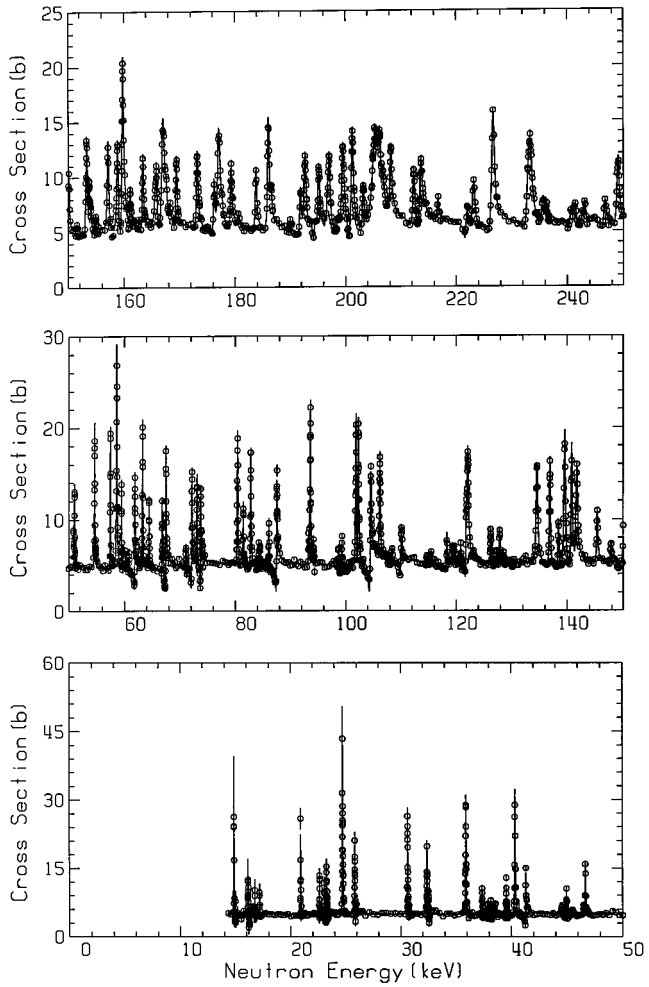

FIG. 1. Total neutron cross sections over selected energy regions. Symbols correspond to experimental measurements and the smooth curves to R-matrix parametrization of the data. Symbols without error bars have errors within the size of the symbol.

to-background ratio. Background sources monitored during the experiment included 2.2 MeV gamma rays from neutron capture in the water moderator, 478-keV gamma rays from the ^{10}B $(n,\alpha\gamma)$ reaction, delayed pulses within the photo tube and scintillator, and a constant beam-independent background. A discussion of these and other experimental details may be found elsewhere [12].

The transmission was then computed from the background-corrected sample-in and sample-out ratio, normalized to the corresponding neutron monitor counts.

III. RESULTS

As a representative sample of the results for ^{124}Sn, Fig. 1 shows the energy range 14–250 keV. The cross sections represented are per atom of tin in the sample. The uncertainties on the data are shown as vertical lines or are less than the size of the symbols. The solid line represents the R-matrix parametrization of the total cross section discussed in the next section.

Strong interference patterns are seen at 88 and 104 keV, characteristic of s-wave interaction. The large non-s-wave resonance at 204 keV, appropriately corrected for the ^{124}Sn abundance, is seen to have a peak-to-valley cross section of 12 b. This must be due to $p_{1/2}$ interaction because the peak cross section at this energy is approximately 13 b for interactions having a spin statistical factor $g_J=1$. Resonances this broad having $g_J=2$, like $p_{3/2}$, would have peak cross sections of 26 b. The narrower resonances at 186 and 226 keV have been assigned to be $p_{3/2}$ on the basis of interference asymmetry. In this way the J^π values are established for the larger resonances. Since impurity isotopes represented approximately 26% of the target, their contributions to the cross section are not insignificant. For low neutron energies the contribution to the cross section is primarily due to the s-wave interaction. We have thus included off-resonance s-wave contributions to the cross section due to $^{116-120,122}$Sn, the largest impurity components. At 50–100 keV neutron energies, for example, this contribution to the background cross section amounts to approximately 1.5 b while that due to the ^{124}Sn is 3.8 b. The significance of this effect on the analysis will be seen in connection with the discussion of the external R functions in Sec. V. Off-resonance contributions for other partial waves of the impurity components are small at these energies in comparison to the s waves and have been ignored. The resonance contributions to the cross sections from the impurity isotopes will be negligible for all but those of very large width. We have assumed that small resonances observed with broad structure are due to strong resonances in the impurity isotopes and have made no attempt to fit those structures.

The early transmission measurements [13] observed a total of five resonances in this isotope up to a neutron energy of 10 keV. In the present case we have extended the energy range to 315 keV, and the number of resonances to 182. From the multilevel resonance analysis we have obtained spin-separated resonance and non-resonant parameters. We have made parity and spin assignments for many of the observed resonances, where earlier results were only able to distinguish s-wave resonances. Besides the normally reported strength functions and level spacings, our R-matrix analysis yields average properties describing the aggregate effect of resonances outside the region as deduced from their influence in the region through observed resonance asymmetries. We deduced these parameters for the $s_{1/2}$, $p_{1/2}$, and $p_{3/2}$ partial-wave components by requiring the asymmetries of the known-spin resonances to be reproduced. This knowledge aided in the assignment of spins to smaller resonances through its influence upon their asymmetries. Since the external R function is related to the real part of the optical-model potential, we are able to deduce some of the parameters of this potential, extending previous investigations [14] of the l dependence of the real well depth of the optical-model potential. In addition parameters of the R function are also used to calculate the potential scattering radii for individual partial-wave interactions.

Table II[7] gives the resonance parameters for $n+^{124}$Sn. The J values in parentheses represent uncertain spins. We have analyzed 182 resonances up to an energy of 315 keV, where resonances were being missed, spin assignments became more uncertain and the multiplet structure too complex to unambiguously decouple. There are regions where the data would support additional small resonances, but we have not been able to determine if these are due to impurity reso-

TABLE II. *R*-matrix resonance parameters for $n+^{124}$Sn for the energy range 14–315 keV.

Energy (keV)	J^π	$g\Gamma_n$ (eV)	$g\gamma_n^2$ (eV)	Energy (keV)	J^π	$g\Gamma_n$ (eV)	$g\gamma_n^2$ (eV)	Energy (keV)	J^π	$g\Gamma_n$ (eV)	$g\gamma_n^2$ (eV)
14.862	$(1/2)^-$	8	554	87.602	$3/2^-$	8	46	179.224	$1/2^-$	134	325
14.977	$(3/2)^-$	1	48	93.261	$1/2^-$	19	108	180.549	$(1/2)^-$	18	43
16.138	$(3/2)^-$	3	204	93.576	$3/2^-$	138	762	183.736	$(1/2)^-$	157	371
16.745	$(3/2)^-$	2	146	94.144	$(3/2)^-$	9	49	185.976	$3/2^-$	323	752
17.180	$(3/2)^-$	3	156	98.646	$(1/2)^-$	15	75	186.492	$(1/2)^-$	34	80
20.913	$(3/2)^-$	10	426	99.236	$1/2^+$	14	14	191.781	$3/2^-$	126	284
22.621	$(3/2)^-$	5	188	101.864	$3/2^-$	169	833	192.616	$1/2^-$	247	552
23.032	$(3/2)^-$	2	85	102.273	$3/2^-$	150	733	194.388	$1/2^+$	56	40
23.238	$1/2^+$	4	8	104.300	$(3/2)^-$	14	67	195.102	$3/2^-$	171	376
23.305	$(1/2)^-$	1	43	104.472	$1/2^+$	129	127	196.970	$1/2^-$	289	630
24.731	$(1/2)^-$	22	774	106.191	$1/2^-$	114	533	198.618	$(3/2)^-$	38	83
25.829	$(3/2)^-$	12	404	108.346	$(3/2)^-$	17	76	199.463	$1/2^-$	409	878
30.628	$(3/2)^-$	25	642	110.009	$1/2^+$	32	30	200.797	$1/2^+$	50	36
32.383	$(1/2)^-$	12	275	110.157	$(1/2)^-$	12	52	201.185	$3/2^-$	303	644
32.497	$(3/2)^-$	4	98	114.623	$1/2^+$	6	6	203.104	$3/2^-$	133	280
35.848	$(1/2)^-$	4	91	115.250	$1/2^+$	8	7	205.339	$1/2^-$	1304	2705
35.906	$3/2^-$	35	708	118.273	$1/2^+$	17	16	206.109	$3/2^-$	134	276
37.358	$(3/2)^-$	7	138	118.280	$(1/2)^-$	21	86	206.675	$(3/2)^-$	34	70
37.883	$(3/2)^-$	2	44	119.315	$(3/2)^-$	23	94	207.650	$(1/2)^-$	50	102
38.159	$(1/2)^-$	1	20	119.594	$(1/2)^-$	17	68	208.118	$3/2^-$	174	355
38.561	$(1/2)^-$	4	68	120.819	$(1/2)^-$	17	68	212.258	$(1/2)^-$	176	351
39.518	$1/2^+$	2	3	121.742	$1/2^+$	44	40	213.541	$1/2^-$	236	467
39.556	$(1/2)^-$	6	108	122.085	$1/2^-$	193	755	216.616	$(1/2)^-$	33	65
40.344	$1/2^-$	44	760	126.205	$(1/2)^-$	36	135	221.802	$1/2^+$	67	45
41.301	$1/2^+$	14	22	127.325	$(3/2)^-$	16	59	223.044	$(1/2)^-$	149	281
44.577	$(3/2)^-$	6	88	127.836	$(1/2)^-$	39	145	226.552	$3/2^-$	592	1098
44.906	$1/2^+$	3	4	128.500	$(1/2)^-$	5	18	232.989	$1/2^-$	505	907
44.979	$(1/2)^-$	6	90	134.544	$1/2^-$	234	809	233.333	$(3/2)^-$	161	289
46.504	$(1/2)^-$	3	47	136.608	$1/2^+$	19	16	235.496	$(1/2)^-$	69	123
46.676	$(3/2)^-$	28	390	136.918	$3/2^-$	156	529	240.399	$1/2^+$	60	39
50.854	$(1/2)^-$	8	106	138.407	$3/2^-$	81	270	241.237	$(1/2)^-$	39	67
51.036	$(3/2)^-$	24	296	139.445	$1/2^+$	46	39	243.002	$(1/2)^-$	70	119
54.641	$1/2^-$	39	447	139.498	$1/2^-$	297	982	243.851	$1/2^+$	27	17
54.834	$(1/2)^-$	5	60	140.755	$3/2^-$	231	753	246.670	$1/2^-$	98	165
57.463	$3/2^-$	52	555	141.681	$1/2^-$	225	729	248.900	$1/2^-$	266	443
58.617	$1/2^-$	91	937	145.366	$1/2^-$	90	284	249.155	$(3/2)^-$	42	70
59.468	$(1/2)^-$	24	240	147.821	$(1/2)^-$	33	102	250.901	$1/2^+$	52	33
59.680	$1/2^+$	4	5	150.093	$(1/2)^-$	93	279	253.737	$1/2^-$	214	348
60.133	$(1/2)^-$	1	10	153.103	$1/2^+$	18	14	255.318	$(3/2)^-$	48	77
60.820	$(1/2)^-$	6	59	153.310	$1/2^-$	172	505	265.391	$1/2^-$	214	332
61.845	$1/2^+$	35	44	153.709	$1/2^-$	79	233	266.226	$(1/2)^-$	106	164
62.953	$(3/2)^-$	4	33	154.033	$1/2^-$	18	54	269.779	$1/2^-$	136	207
63.257	$1/2^-$	55	508	154.774	$1/2^+$	19	15	273.290	$3/2^-$	241	362
64.413	$(1/2)^-$	25	222	157.099	$1/2^-$	205	584	274.616	$1/2^-$	303	453
66.784	$(1/2)^-$	23	201	158.811	$1/2^-$	224	631	276.955	$1/2^+$	144	87
66.951	$(3/2)^-$	15	128	159.698	$1/2^-$	348	975	277.400	$3/2^-$	42	62
67.422	$1/2^+$	51	62	159.778	$3/2^-$	130	364	279.515	$(1/2)^-$	198	290
71.050	$(3/2)^-$	8	67	160.500	$1/2^-$	4	11	284.522	$(3/2)^-$	131	188
72.120	$1/2^+$	46	54	160.967	$1/2^+$	46	36	285.367	$1/2^-$	444	636
73.066	$(1/2)^-$	41	311	162.743	$(1/2)^-$	31	86	287.905	$(3/2)^-$	182	258
73.717	$1/2^+$	37	43	163.334	$3/2^-$	151	411	289.101	$1/2^-$	1054	1489
80.261	$1/2^+$	4	4	165.571	$(1/2)^-$	73	195	289.173	$(3/2)^-$	202	285
80.403	$1/2^-$	81	546	165.790	$1/2^-$	120	321	298.716	$1/2^-$	504	688
81.447	$(1/2)^-$	32	215	166.960	$1/2^-$	484	1283	299.061	$(3/2)^-$	206	280
82.784	$1/2^-$	72	468	167.515	$(3/2)^-$	36	95	307.340	$1/2^-$	611	808
82.927	$(3/2)^-$	3	16	168.230	$(1/2)^-$	20	53	309.452	$1/2^+$	160	91
84.240	$(1/2)^-$	11	72	169.354	$(3/2)^-$	135	352	310.625	$(3/2)^-$	269	351
84.457	$(1/2)^-$	9	59	173.133	$1/2^-$	190	483	312.955	$1/2^+$	146	83
86.051	$(3/2)^-$	20	122	176.158	$3/2^-$	113	282	314.264	$(3/2)^-$	391	505
86.108	$(3/2)^-$	15	94	177.034	$1/2^-$	410	1014	314.745	$(3/2)^-$	140	181
87.472	$1/2^+$	60	65	177.622	$(3/2)^-$	21	51				

nances or weak multiplet structure. Their inclusion would only significantly impact the level spacing and not the strength. We have thus ignored them. By extending the energy range of the analysis to include more resonances in each spin group we have been able to reduce the uncertainty of the very low s-wave strength function and provide the strengths and level spacings of the p-wave interactions. The values for the widths come from integer rounding of the actual values. The values for the small-width resonances may thus differ significantly from the actual results. The actual values, together with the entire spectrum of resonances and the deduced neutron resonance parameters have been transmitted to the National Nuclear Data Center at Brookhaven National Laboratory. Errors on these widths are approximately 5, 10, and 20 % for the largest, intermediate, and smallest peak height resonances, respectively. The energy uncertainties are one-fifth of the neutron energy resolution given in Sec. II.

IV. *R*-MATRIX ANALYSIS

Here we will only discuss the part of the formalism containing parameters deduced from the fitting process. A detailed description of the R-matrix formalism used in the analysis was presented in a previous paper [1]. For other details of the model one is referred to Sec. IV in that work.

The R function has been expressed as a sum over the observed resonances plus a smoothly increasing function of energy which describes the aggregate effect of levels external to the region of measurement,

$$R_{lJ}(E)=\sum_{\lambda=1}^{N}\frac{\gamma_{\lambda lJ}^2}{E_{\lambda lJ}-E}+R_{lJ}^{\mathrm{ext}}(E), \tag{1}$$

where γ_{lJ}^2 and E_{lJ} are free parameters representing the reduced width and energy of the λth resonance, with the γ_{lJ}^2 related to the observed neutron widths, Γ_n, by the relation,

$$\gamma_{lJ}^2=\frac{\Gamma_{nlJ}}{2P_l}, \tag{2}$$

where P_l is the neutron penetrability. The external R function influences both the off-resonance cross section and the interference asymmetry of individual resonances and is a measure of the average effect of resonances in the vicinity but outside of the analyzed region. This part of the R function contains parameters that are adjusted in fitting the features of the cross section which this function influences. We write this part of the R function as

$$R_{lJ}^{\mathrm{ext}}(E)=\overline{R}_{lJ}-\tilde{s}_{lJ}\ln\left[\frac{E_{\mathrm{up}}-E}{E-E_{\mathrm{lo}}}\right], \tag{3}$$

with the smooth function, $\overline{R}_{lJ}$, parametrized as

$$\overline{R}_{lJ}(E)=\alpha_{lJ}+\beta_{lJ}E \tag{4}$$

and α_{lJ} andβ_{lJ} being free parameters. The log term accounts for resonances just outside the experimental region, $[E_{\mathrm{lo}}, E_{\mathrm{up}}]$. The $\tilde{s}_{lJ}$ represent the strength outside the region and are assumed to be continuously distributed. We have made the reasonable assumption that this strength is equal to the strength function, $\langle\gamma_{lJ}^2\rangle/D_{lJ}$, observed within $[E_{\mathrm{lo}}, E_{\mathrm{up}}]$, where D_{lJ} is the observed average level spacing. Thus the R-matrix analysis of total neutron cross sections results in two average measures of the interaction, the strength which is related to the imaginary part of the optical potential, and the R^{ext} which is related to the real part of the potential. This parametrization facilitates the averaging of the scattering function for comparison to an optical model as discussed in Sec. VI of [1].

In comparison of experiment and theory it is critical that both use a common boundary or channel radius [15]. The calculated strength function, for example, is dependent upon this quantity and the dependence is especially important for other than s waves. The same is true for the smooth R function. We have thus used a boundary radius of $1.45\times A^{1/3}$ fm in calculating penetrabilities and hard-sphere phase shifts, for all partial waves, and for the model calculations as well. The final R-matrix parameters which best described the observed transmissions were determined by solving Bayes' equations using the R-matrix code SAMMY [16]. The fitting procedure included resolution broadening of the transmissions and Doppler broadening of the calculated cross sections, with an effective thermal temperature for the nucleus of 306 K.

The s-wave resonances are easily distinguished by their characteristic asymmetry. We have assumed all other resonances to be due to p-wave interaction because of the small probability of d-wave interaction in this energy range. Three bases determined the p-wave spin assignments: (1) for resonances with widths larger than the resolution width the peak-to-valley cross section for $p_{3/2}$ is two times that for $p_{1/2}$; (2) resonances with widths comparable to the resolution width manifest resonance-potential scattering interference asymmetry which decreases with increasing l value; (3) resonances with smaller width manifest resonance-resonance interference only if near a strong resonance of the same J^π. We used an iterative procedure to determine most of the J^π assignments, requiring the final assignment to provide a good description of the asymmetry patterns which arise from both resonance-resonance and resonance-potential scattering interference. The latter asymmetry serves to also determine the R^{ext} parameters for each partial wave for which there are one or more resonances manifesting sufficient asymmetry (in this case $s_{1/2}, p_{1/2}, p_{3/2}$). This is possible even in the case where only one large resonance exists in the region of analysis.

V. AVERAGE PROPERTIES

Resolved-resonance analysis of neutron total cross-section data results in three average quantities characterizing the interaction. In cases where the energy range of analysis is sufficient, their functional form can be determined. These functionals are the strength function, the level spacing and an external R function which characterizes the average properties outside the energy region of analysis. Two of these can be modeled by an optical potential and the other by statistical models of nuclear structure. With ORELA data we are generally able to determine these quantities for each partial wave participating in the interaction and thus provide constraints for the parameters of the nuclear models used to describe

them. We will define and treat each of these properties in turn.

A. Strength functions

From a plot of the cumulative reduced neutron width [see Eq. (2)] versus neutron energy we can determine the R-matrix strength functions, $\tilde{s}_{lJ}$, through the slope of the histogram in cases where the strength is independent of energy. In Fig. 2 we have plotted the quantity

$$g_J\gamma_\lambda^2, \tag{5}$$

where γ_λ^2 is the reduced neutron width of the λth resonance and l is the orbital angular momentum quantum number. The corresponding slopes are related to the strengths of each of the angular momentum states. Results for both s and p waves are shown here to emphasize the great difference in s and p strengths for this nuclide. The ratio of the slopes or strengths was 15, essentially the same as for ^{122}Sn. The only difference is that the sum for p waves was 10% greater for ^{122}Sn. Both these isotopes thus have strikingly similar strength distributions.

A single line passed through the histograms would sufficiently describe the trend over the entire energy range, indicating a constant strength. Our s-wave assignments are unambiguous and the increase near 200 keV in the p-wave histogram must represent statistical fluctuations if we assume low probability of d-wave interaction in this energy range. The total p-wave strength is calculated from the expression

$$\tilde{s}_l=\frac{\Sigma_{\lambda J}\, g_J\gamma_\lambda^2/(2l+1)}{\Delta E_l}, \tag{6}$$

to be $(5.6\pm0.7)\times10^{-2}$. This value is in good agreement with the trends in this mass region but 30% below predictions of a deformed optical model calculation [17]. The value is 12% lower than the result for ^{122}Sn. The value for the s-wave strength function is $(3.8\pm1.0)\times10^{-3}$, an order of magnitude lower than that for the p waves but consistent with results for other isotopes of tin and with theoretical investigations of nuclear structure in this mass region. The result is identical with that for ^{122}Sn. The corresponding values for s and p waves, in conventional units are $(0.12\pm0.03)\times10^{-4}$ and $(1.8\pm0.2)\times10^{-4}$, respectively.

With the present data we are able to establish the strength for each partial wave by the slopes of the plots of just the cumulative reduced widths, without the statistical weighting factors. These are presented in Fig. 3 for the p waves. As discussed in the companion paper, there is an element of uncertainty in the apportionment of small resonances among the two spin states. In that work the two p-wave spin groups had comparable strengths with the $p_{1/2}$ being somewhat larger. Here, we find the strength for the $p_{1/2}$ component exceeding that of the $p_{3/2}$ by almost a factor of 4. This behavior is not explained by the current work, but has been noted in other nuclei. The magnitude of the enhancement of the $p_{1/2}$ strength over the $p_{3/2}$ for this nucleus makes a strong case for this being a real effect in this isotope of tin.

We found the spin dependence of the p-wave strength to persist when only including unambiguous $p_{1/2}$ and $p_{3/2}$ resonances in the samples, the enhancement even increasing by 15%. As in the ^{122}Sn study we also established upper limits for the average parameters, for each partial wave, by including all resonances of indefinite J^π in each of the spin groups, separately. Each of the p-wave spin groups constructed in this manner have 65–80 % of the resonances indefinite with approximately 30–50 % of the resulting strength attributable to these uncertain resonances. Average resonance parameters, their statistical uncertainties, and their upper and lower limits are presented in Table III in conventional units. The R-matrix strength functions, $\tilde{s}_{lJ}$, are discussed Sec. V C. By careful analysis of larger samples we have reduced the uncertainty on the s and p-wave strength functions and level spacings, the number of resonances in this study representing a 20-fold increase over that of Mughabghab's tabulation [18].

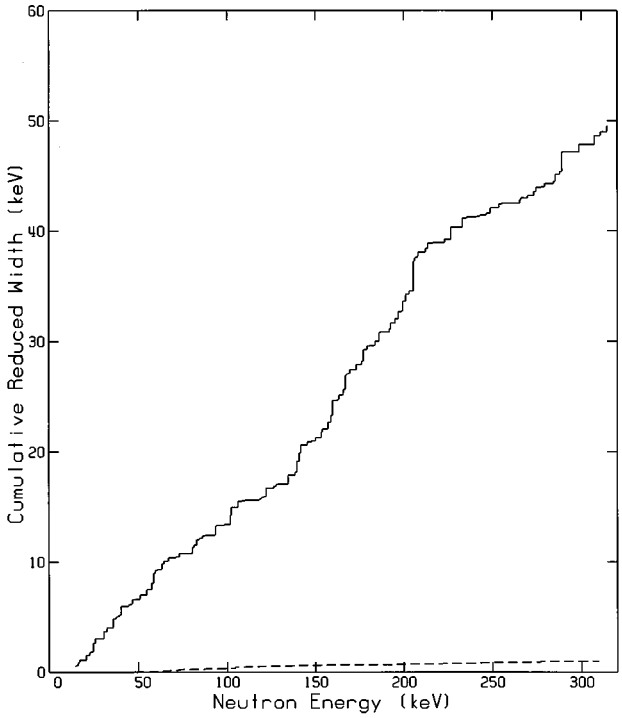

FIG. 2. s- and p-wave strength functions. The cumulative values for the p waves (solid histogram) represent that of Eq. (5) for a channel radius of 7.23 fm. The sum for s waves is only ≈1 keV.

B. Level spacings

We have plotted in Fig. 4 the cumulative number of levels for each spin group. We observed 32 s-wave resonances (----) up to an energy of 315 keV. From this histogram, above an energy of 250 keV, it would appear that small resonances are being missed. This is likely due to their small widths and interference with other resonances. This would have a greater effect on the level spacings than on the strength function. The level spacings listed in Table III are calculated from the number of levels and the energy range. If one uses instead the slopes of individual histograms in Fig. 4, the spacings obtained are bracketed by the tabulated values and the lower limits given in Table III.

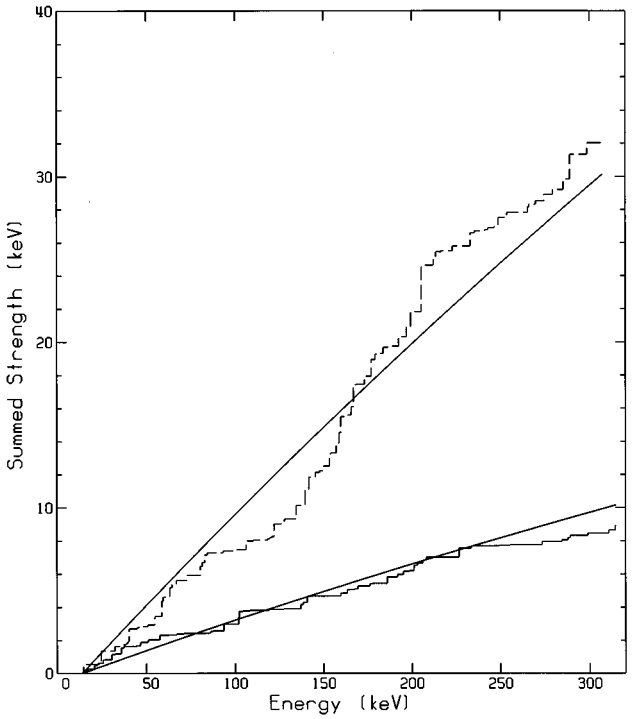

FIG. 3. Strength functions for p-wave components. The dashed histogram is for the $p_{1/2}$ partial wave. The slopes of these histograms give the corresponding strength functions. The solid lines represent optical-model fits, discussed in Sec. VI.

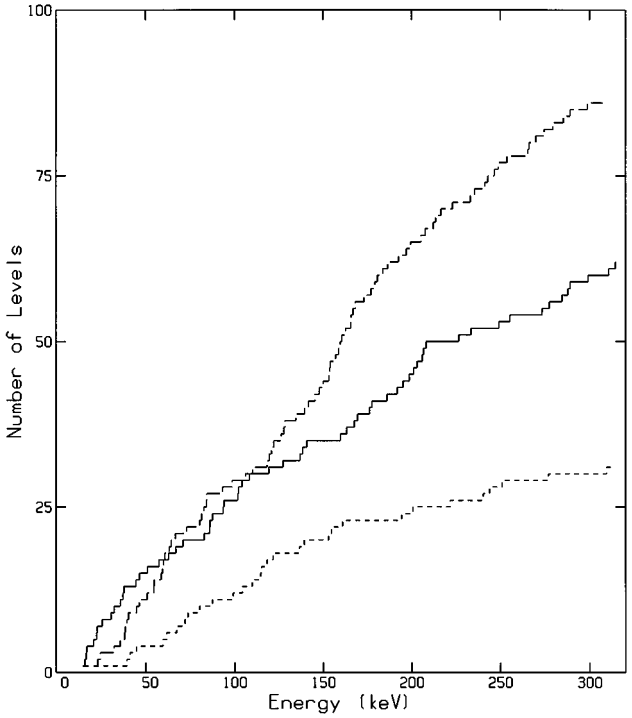

FIG. 4. Cumulative number of levels vs neutron energy for the $s_{1/2}$ (---), $p_{1/2}$ (––), and $p_{3/2}$ (—) resonances. The slope of the histograms gives the level density for that partial wave.

For ^{122}Sn the $p_{1/2}$ strength exceeded that for $p_{3/2}$. In the present case this is true for the number of levels as well. The expected $2J+1$ dependence is reversed. The number of $p_{1/2}$ and $p_{3/2}$ resonances unambiguously established by peak height and interference asymmetries is 41 and 22, respectively. For both the strength and level density of these two groups, the anomaly is greater for the definite-spins grouping than when using the spins indicated in Table II. The indefinite spins given in Table II were established simply on the basis of small χ^2 differences in the resonance-fitting process for different assumed spins. For the expected $2J+1$ distribution of levels to be reflected in these spin groups would require that 90% of all uncertain resonances be assigned to the $p_{3/2}$ spin group. It is unlikely that a χ^2 minimization process would consistently favor one spin over the other when the differences are too small to be conclusive. It would therefore appear that this result is fundamental and we may be seeing an important breakdown of the $(2J+1)$ law.

TABLE III. Average resonance parameters for ^{124}Sn+n.

No. obs.	J^π	$S_J^l(\times 10^{+4})$	D (keV)
32	s	0.12 (3)[a]	9.3 (9)
150	p	1.8 (2)	2.0 (1)
87	$p_{1/2}$	3.5 $(6)^{4.2a}_{3.0}$	3.4 $(2)^{6.7}_{2.4}$
63	$p_{3/2}$	0.9 $(2)^{1.3}_{0.7}$	4.8 $(3)^{11.5}_{2.8}$

[a]In our notation, 0.12 (3) is equivalent to 0.12 ± 0.03 and 3.5 $(6)^{4.2}_{3.0}$ indicates that upper and lower limits are 4.2 and 3.0, respectively as discussed in the text. The numbers in parentheses represent statistical uncertainties.

C. External R functions ($R^{\rm ext}$)

The $R^{\rm ext}$ are related to the real part of the optical potential and their general energy trends provide constraints on the optical-model parameters. The $R^{\rm ext}$ parameters are established through resonance asymmetries and background contributions of each partial wave. Physically this function represents the resonance-potential scattering interference due to resonances outside the analyzed energy region. Since we have resonances of each J^π distributed throughout the energy range we have been able to deduce the energy dependence of this function. At low energies, where the contribution to the off-resonance cross section is almost entirely due to s-wave potential scattering, the s-wave smooth R function is related to the potential scattering radius R_0' by

$$R_0' = a_c[1-\overline{R_0}(E=0)], \tag{7}$$

where $\overline{R_0}$ is evaluated for $E=0$. The $\overline{R_0}$ obtained from fitting is dependent on the choice of channel radius, a_c, but the value for R_0' is independent of that parameter. The s-wave $R^{\rm ext}$ parameters are therefore well determined in this energy region through their influence upon the potential scattering radius and thus the background cross section. A 10% change in the s-wave $R_0(E=0)$, for example, produces a visually distinguishable change in the total cross section throughout the low-energy region. The increasing contribution of other partial waves to the off-resonance cross-section results in a

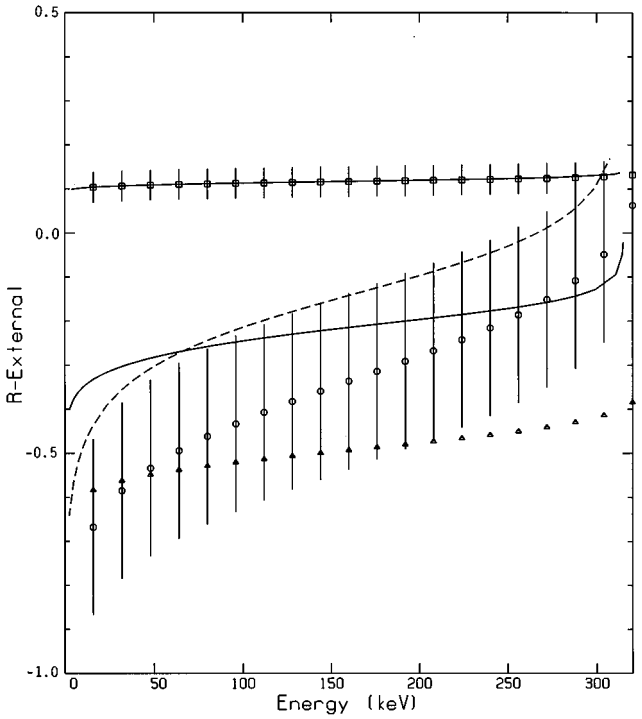

FIG. 5. The external R functions for the $s_{1/2}$ (□), $p_{1/2}$ (⊙), and $p_{3/2}$ (△) partial waves. The error bars for the $p_{3/2}$ are one-half those shown for the $p_{1/2}$. Smooth curves represent optical-model predictions (dashed curve for $p_{1/2}$).

maximum uncertainty for this parameter for s waves, for the entire energy region, of 25%. Since we have greater percentages of impurity components in this sample than in the ^{122}Sn, the inclusion of their contributions is essential to a correct determination the R^{ext} parameters for ^{124}Sn. We have calculated values for the constant α [see Eq. (4)] for each of the impurity isotopes from the R_0' values of Mughabghab and have held them constant. We have set the β values to zero. Similarly, values for the R-matrix strengths $\tilde{s}_0$ have been calculated from Mughabghab's conventional strengths as

$$S^0 = 4.4\times 10^{-4}\,\frac{A}{A+1}\,a_c\tilde{s}_0, \tag{8}$$

for a channel radius $a_c = 7.23$ fm.

We established the R^{ext} uncertainties for p waves by manual variation of the parameter α until a visual comparison showed noticeable disagreement with those asymmetries and nonresonant cross sections obtained from least-squares parameters, in a region where the largest resonance(s) of a given J^π occurred. Changes of 100% are required in the low-energy region and 20% for the upper energy region. We have taken this uncertainty to be constant at approximately 60% of the value at the middle of the energy region. For clarity, p-wave error bars are shown in Fig. 5 for only the $p_{1/2}$. Those for the $p_{3/2}$ were 50% of the magnitude shown for the $p_{1/2}$ case. The ^{124}Sn-R^{ext} parameters for the contributing partial waves are given in Table IV where the uncertainties in α and β are reflected through the value of the

TABLE IV. Parametrization [see Eq. (4) for relationship of parameters to the external R function] for the external R functions.

A	J^π	α	β (1/MeV)	$\tilde{s}_{lJ}(\times 10^{+2})$	$\overline{R(E)}$
124	$s_{1/2}$	0.11	0.013	0.38(10)[a]	0.12 (3)
124	$p_{1/2}$	−0.35	0.10	$11(2)^{13}_{9}$	−0.33(20)
124	$p_{3/2}$	−0.50	0.07	$3.0(6)^{4.1}_{2.1}$	−0.49(10)
116	$s_{1/2}$	0.14		0.40	0.14
117	$s_{1/2}$	0.11		0.65	0.11
118	$s_{1/2}$	0.17		1.45	0.17
119	$s_{1/2}$	0.17		0.32	0.17
120	$s_{1/2}$	0.11		0.40	0.11
122	$s_{1/2}$	0.21		0.38	0.21

[a]In our notation, 0.38 (10) corresponds to 0.38±0.10, etc., α and β uncertainties are discussed in the text. Upper and lower limits are established as in Table III.

smooth R function, $\overline{R_{lJ}}$, at the midpoint of the energy region. For completeness the parameters used for the impurity isotopes are included. The upper and lower limits indicated for the R-matrix strength, $\tilde{s}_{lJ}$, have been determined as discussed in Sec. V A.

VI. AVERAGE PARAMETERS AND THE OMP

Detailed, resolved-resonance analysis of the ^{124}Sn+n system has permitted determination of the R_{lJ}^{ext} and $\tilde{s}_{lJ}$ and their energy dependencies. These functions have been shown to be sufficient to construct energy-averaged scattering functions which can be compared with those predicted by an optical model. In this prescription [19] the complex R function used to form the scattering function can be simply expressed in terms of the smooth R function and the strength deduced in the analysis as

$$R_{lJ}(E) = \overline{R_{lJ}}(E) + i\pi\tilde{s}_{lJ}(E). \tag{9}$$

For more detail concerning the comparison of the averaged empirical scattering functions with the predicted $S_{lJ}^{\text{OMP}}(E)$, one should consult Johnson *et al.* [20].

As in the previous paper on Sn, we used the standard prescription for the Woods-Saxon potential and performed a least-squares adjustment of the real and imaginary depths until the integrated strengths and the R^{ext} predicted by the model agreed with our experimental values over the analyzed region. Each partial wave has been treated separately to determine if our results warrant any spin or parity dependence in the optical-model potential parameters. The geometry of the model used was taken from work on ^{116}Sn and ^{120}Sn by Guss *et al.* [21] and held constant at the values

TABLE V. Radius and diffuseness parameters (values are all in fm) for OMP.

	V_r	W_D	V_{SO}
r	1.23	1.25	1.12
a	0.66	0.54	0.50

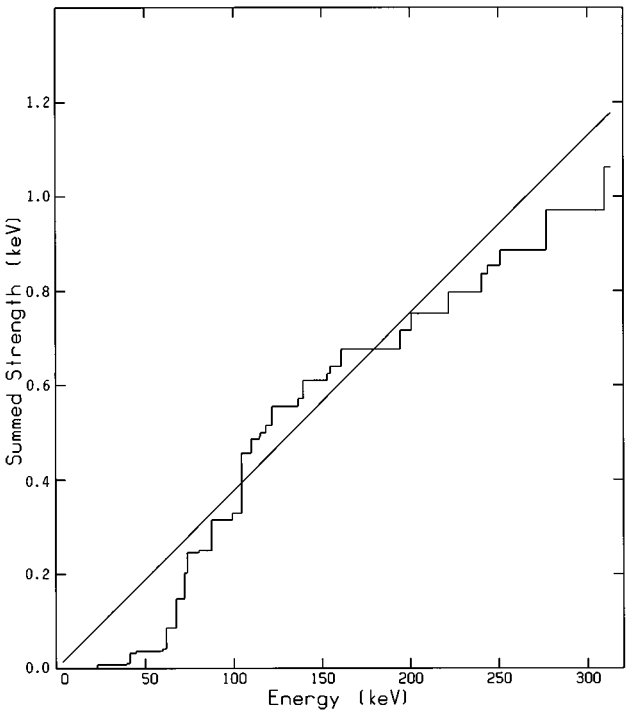

FIG. 6. Experimental integrated s-wave strength and model predictions, based upon geometric and potential parameters in Tables V and VI.

shown in Table V. The well depth for the spin-orbit potential was also held constant in the fitting process.

The comparison between model and empirical R^{ext} is shown for each of the participating partial waves in Fig. 5. The topmost solid curve for the s-wave R^{ext} is in excellent agreement with the empirical values. For the p waves, however, the predicted results are systematically high throughout most of the region, but display the expected energy dependence. (For the p waves the dashed curve is to be compared with the $\odot$ values and the solid curve with the Δ values.) The error bars for the $p_{3/2}$ are not shown but are one-half those for the $p_{1/2}$. Despite its smaller uncertainty the $p_{3/2}$ partial wave is seen to be more poorly represented by the model predictions. These functions are more sensitive to changes of the real part of the optical potential and thus have a greater influence upon the parameters of this potential. We have not been able to find a single potential depth that will model both s- and p-wave R^{ext} functions. This suggests that an l dependence for the potential depth is necessary to model this average property of the ^{124}Sn nucleus.

TABLE VI. Spherical optical-model parameters (well depths are in MeV).

	Present work			Guss *et al.*	
	V_r	W_D	V_{SO}	V_r	W_D
$s_{1/2}$	45.1	0.9	6.5	47.9	0.9
$p_{1/2}$	48.0	6.0	6.5	47.9	0.9
$p_{3/2}$	49.4	2.5	6.5	47.9	0.9

On the other hand, the strength function is more strongly influenced by the surface imaginary depth, W_D, of the optical potential. The fitting process to determine the optimum potential parameters involved a comparison of model and empirical results. The depths of both potentials were adjusted in simultaneously fitting both average quantities, for each partial wave. Again, we were unable to obtain common potential parameters for all the partial waves. The result, for the $s_{1/2}$ integrated strength is presented in Fig. 6. While one could imagine two regions of distinctly different slopes, changing at approximately 150 keV the single slope of the model is more consistent with the weak strength observed for the Sn isotopes and in this mass region.

Results for the separate least-squares fitting of the component p-wave integrated strengths are indicated by the solid lines in Fig. 3. These are seen to describe the data well over the entire energy range. However, the 300% difference in the summed strengths requires a difference in the depths of the surface imaginary potential required to describe these component strengths. In the case of ^{122}Sn the summed $p_{1/2}$ strength was only 30% greater than that of the $p_{3/2}$ and the same potential parameters were able to describe both p-wave component strengths.

We are the only group investigating the optical-model potential through low-energy neutron interactions with the ability to provide directly deduced, spin-separated potential well depths. Some who deduce optical-model potential parameters from energy averaged total or scattering cross sections include strength functions and potential scattering radii for s, p, and d waves as parameters of the least-squares analysis. One would expect the two approaches to agree in an average

TABLE VII. Optical-model parameters describing present results, for various geometries. α_V and α_D give the energy dependence of the corresponding well depths.

	Guss[a]			Harper[b]			Rapaport[c]		
	$s_{1/2}$	$p_{1/2}$	$p_{3/2}$	$s_{1/2}$	$p_{1/2}$	$p_{3/2}$	$s_{1/2}$	$p_{1/2}$	$p_{3/2}$
V_r (MeV)	45.1	48.0	49.4	44.3	46.8	48.3	46.9	49.2	52.1
W_D (MeV)	0.9	6.0	2.5	1.7	8.2	3.5	0.6	6.2	3.1
V_{SO} (MeV)	6.5	6.5	6.5	5.5	5.5	5.5	6.2	6.2	6.2
α_V (MeV^{-1})		0.30			0.27			0.36	
α_D (MeV^{-1})		0.0			0.053			0.52	

[a] r_V=1.23, r_D=1.25, r_{SO}=1.12, a_V=0.66, a_D=0.54, a_{SO}=0.50, all in fm.
[b] r_V=1.26, r_D=1.26, r_{SO}=1.12, a_V=0.58, a_D=0.40, a_{SO}=0.50, all in fm.
[c] r_V=1.20, r_D=1.32, r_{SO}=1.01, a_V=0.70, a_D=0.62, a_{SO}=0.76, all in fm.

TABLE VIII. Strengths and potential scattering radii for ^{124}Sn.

J^π	Present	Timokhov *et al.*	Popov *et al.*
S_0	0.12 (3)$\times 10^{-4}$	0.1 (7)$\times 10^{-4}$	
S_1	1.8 (2)$\times 10^{-4}$	1.6 (2)$\times 10^{-4}$	3.5 (3)$\times 10^{-4}$
R_0'	6.4 (2)	5.9 (2)	5.5 (1)
R_1'	10.5 (3)	9.9 (3)	8.6 (2)

sense. In fact, the results for our s- and p-wave potential parameters are seen to bracket the parameters found for similar isotopes of tin in the study of Guss *et al.* [21], after suitable adjustments for isotope and energy differences. The parameters for our model are presented in Table VI with the values from the model deduced by Guss *et al.* It was noted that their model overestimated the p-wave strength functions by more than 40%. When we used the geometry and well depths of Guss *et al.*, both our model R^{ext} and integrated strength was too high for s waves by a factor 2. For $p_{1/2}$ the model R^{ext} was equivalent to the measured one at low energy but had the wrong energy dependence. The strength for this component was low by the factor 2. For the $p_{3/2}$ component the R^{ext} was 50% too high and the integrated strength was 50% below that observed.

Where significant numbers of resonances of differing spin can be identified, low-energy resolved-resonance analysis provides information on the optical-model potential that is not available from cross-section analyses in the MeV energy region. In the present study, as in other similar studies [14], we must conclude that the real well depth must be deeper for p waves than for s waves to describe the low-energy neutron interaction. Also, in this nucleus significant differences in the surface imaginary potential well depths are required to describe the anomalous enhancement of $p_{1/2}$ strength over that for the $p_{3/2}$ interaction.

VII. DISCUSSION

We have sought to ensure that the model geometry could not be responsible for the l dependence of the real well depths for s and p waves by repeating the least-squares search, using geometries deduced in other studies. When we searched for well depths, corresponding to several of these geometries, which would best represent all our data the l dependence persisted in each case. Only the magnitudes of the well depths changed with geometry. Thus it is seen in Table VII that in every case the difference between required s- and p-wave well depths is approximately 3 MeV for the real potential. Though not as pronounced, deeper binding (by 1–3 MeV) is also required for the $p_{3/2}$ component of the p waves. In the ^{122}Sn study the imaginary potentials for the p-wave components were essentially identical. Due to the anomalous behavior of the $p_{1/2}$ component strength in the present study, the imaginary depths differ by as much as 5 MeV. It should be noted that not all features of all data sets of the other studies have been properly described by their deduced parameters. The cross sections are low in some cases and high for others. This could be a manifestation of the need for an l dependence, which our data require.

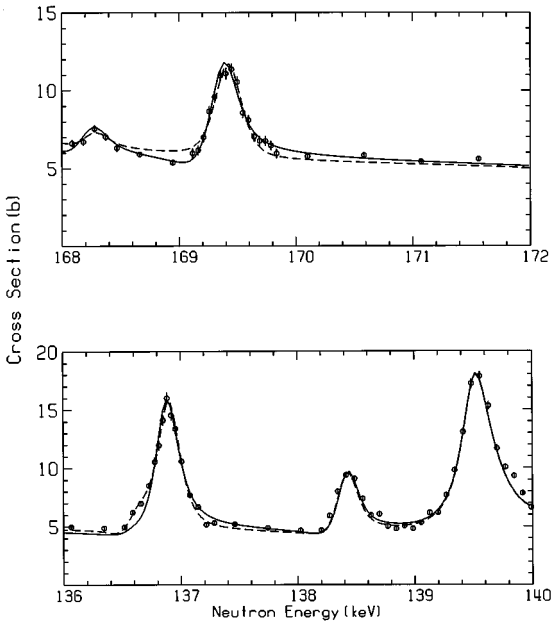

FIG. 7. Total cross-section data for $n+^{124}$Sn and least-squares R-matrix fits for assumed $p_{3/2}$ (solid) and $d_{3/2}$ (dashed) spin assignments, illustrating basis for spin assignments to resonances.

Timokhov *et al.* [22] in a different approach have modeled neutron capture cross sections from 0 to 450 keV and transmissions over the energy range 20–1400 keV, for the stable tin isotopes, in the framework of the Hauser-Feshbach-Moldauer formalism. By expressing the cross sections in terms of the strength functions and potential scattering radii they have deduced these parameters for each isotope. Using the optical model geometry of Harper *et al.* they also determined the real and imaginary depths of an optical-model potential to reproduce their total cross sections and known strength functions. They were then able to calculate potential scattering radii. Only their imaginary well depth differed significantly from that of Harper *et al.* It was noted that the predictions of Harper overestimate the total neutron cross section below 300 keV by as much as 30%, since their data did not extend below that energy. The potential parameters of Timokhov overestimate the total cross section in the energy region 0.2–0.8 MeV by as much as 7%. We have used the well depths from both of these works to describe our data and find that neither will provide an adequate description.

From our smooth R functions we can determine potential scattering radii according to the relation

$$R' = a_c[1 - \overline{R}(E=0)].$$

Comparison with similar quantities deduced by Timokhov *et al.* and Popov *et al.* [23] are presented in Table VIII. We see that the present results are in general agreement with the results deduced by other quite different means. However, the potential parameters necessary to represent the resolved resonance and the average data call for a different real well depth for the different angular momenta. Thus our high-resolution

elastic neutron-scattering data continue to support the notion that one must impose an l dependence to an optical-model description if all the data are to be satisfactorily described.

VIII. CONCLUSION

From our analysis of high-resolution neutron total cross-section data we find numerous indications of anomalous behavior in the $n+^{124}$Sn system: (a) the spherical optical model that will best represent our empirical average scattering functions requires a parity dependence for the depth of the real potential; (b) moreover, the anomalous enhancement of observed $p_{1/2}$ strength suggests a J dependence for the surface imaginary potential depth; (c) instead of a 50/100 ($p_{1/2}/p_{3/2}$) distribution for the 150 p-wave resonances we observe a 87/63 distribution, in clear violation of the $(2J+1)$ law; (d) finally, our spin assignments indicate a parity dependence for the level spacing in this nuclide, as seen in the 87/32 ($p_{1/2}/s_{1/2}$) distribution of resonances. This parity dependence persists even if we use the $(2J+1)$ law in apportioning the 150 p-wave resonances. Calculations [24] of average level spacings for odd and even parity states at excitations near the neutron binding energy have indicated that the even-to-odd ratio, for the same J, can be as high as seven. These predictions have been confirmed [25] in the iron isotopes, where the s-wave strength is very large and in the companion work on ^{122}Sn where the s-wave strength is very small. Similarly, other calculations for ^{63}Cu [26] give a level density ratio ρ^-/ρ^+ of 1.4 at 10 MeV excitation and 1.8 at 20 MeV. The persistence of this effect in ^{124}Sn suggests that caution is warranted in applying the usual assumptions to nuclear level counting at excitations near the neutron separation energy.

These inferences are predicated upon a number of assumptions: (1) the energy range of the analysis is such that we only expect s- or p-wave interactions to occur; (2) all resonances not exhibiting the strong interference asymmetry characteristic of s waves are due to p-wave interactions; and (3) the criterion used in the apportionment of small symmetric resonances into the $p_{1/2}$ and $p_{3/2}$ spin groups should not result in biased samples. To understand the absence of observed d-wave interaction we compare the penetrability factors (see, e.g., p. 19 in Ref. [18]) for p- and d-wave neutrons. At 15 keV the angular momentum barrier would favor p-wave over d-wave penetration by a factor of more than 200. At 300 keV the factor is 9. Since, in addition, the p-wave strength function is an order of magnitude greater than that for s or d waves we expect to see no significant d-wave interaction over the energy range investigated. We have nevertheless attempted d-wave assignments for all non-s-wave resonances. The χ^2 supported only three resonances for possible d-wave assignment. Figure 7 depicts the result of applying $d_{3/2}$ and $p_{3/2}$ fits to peaks at 136.9 and 169.4 keV. The χ^2 values differ by two in each case, the 136.9 keV resonance calling for a $d_{3/2}$ assignment and that at 169.4 keV calling for a $p_{3/2}$ assignment.

These anomalies thus appear real and may simply be a consequence of the position of this $(A=124)$ nuclide near the minimum between the $3S$ and $4S$ size resonances and the maximum of the $3P$ size resonance. To the extent the assumptions are valid, this tin isotope at least provides for potentially rich excogitations.

ACKNOWLEDGMENTS

This work was partially supported by the U.S. Department of Energy under Contract No. DE-FG05-86ER40293 with Middle Tennessee State University. The Oak Ridge National Laboratory is operated by Martin Marietta Energy Systems, Inc. for the Department of Energy under Contract No. DE-AC05-84OR21400.

[1] R. F. Carlton, J. A. Harvey, and N. W. Hill, Phys. Rev. C **52**, 1498 (1995).

[2] J. A. Harvey and T. Fuketa, in *Proceedings of the Conference on Study of Nuclear Structure with Neutrons*, edited by M. Neve de Mervergnies, P. Van Asshe, and J. Vervier (Noth-Holland, Amsterdam, 1966), p. 527.

[3] C. Wong, S. M. Grimes, and R. W. Finlay, Phys. Rev. C **29**, 1710 (1984).

[4] J. Rapaport, M. Mirzaa, H. Hadizadeh, D. E. Bainum, and R. W. Finlay, Nucl. Phys. **A341**, 56 (1980).

[5] J. Rapaport, V. Kulkarni, and R. W. Finlay, Nucl. Phys. **A330**, 15 (1979).

[6] R. W. Finlay, J. Rapaport, M. H. Hadizadeh, M. Mirzaa, and D. E. Bainum, Nucl. Phys. **A338**, 45 (1980).

[7] R. W. Harper, T. W. Godfrey, and J. L. Weil, Phys. Rev. C **26**, 1432 (1982).

[8] R. W. Harper, J. L. Weil, and J. D. Brandenberger, Phys. Rev. C **30**, 14 542 (1984).

[9] V. M. Timokhov, M. V. Bokhovko, A. G. Isakov, L. E. Kazakov, V. N. Kononov, G. N. Manturov, E. D. Poletaev, and V. G. Pronyaev, Sov. J. Nucl. Phys. **50**, 375 (1989).

[10] A. B. Popov, and G. S. Samosvat, in *Proceedings of the International Conference on Nuclear Data for Basic and Applied Science*, edited by P. G. Young, R. E. Brown, G. F. Auchampaugh, P. W. Lizowski, and L. Stewart (Gordon and Breach, New York, 1985), p. 621.

[11] D. C. Larson, N. M. Larson, and J. A. Harvey, N. W. Hill, and C. H. Johnson, Oak Ridge National Laboratory Report No. ORNL/TM-8203, Oak Ridge, Tennessee, 1984, unpublished.

[12] D. C. Larson, N. M. Larson, and J. A. Harvey, Oak Ridge National Laboratory Report No. ORNL/TM-8880, Oak Ridge, Tennessee, 1984, unpublished.

[13] T. Fuketa, and J. A. Harvey, Oak Ridge National Laboratory Report No. ORNL-3425, 1962, unpublished, p. 36.

[14] C. H. Johnson, in *Neutron-Nucleus Collisions*, edited by J. Rapaport, R. W. Finlay, S. M. Grimes, and F. S. Dietrich, AIP Conf. Proc. No. 124 (AIP, New York, 1985), p. 446.

[15] R. F. Carlton, R. R. Winters, C. H. Johnson, J. A. Harvey, and N. W. Hill, Phys. Rev. C **38**, 1605 (1988); C. H. Johnson, R. F. Carlton, and R. R. Winters, *ibid.* C **39**, 415 (1989).

[16] N. M. Larson, Oak Ridge National Laboratory Report No. ORNL/TM-9179/R2, 1989, unpublished.

[17] S. F. Mughabghab, in *Neutron Cross Sections and Technology*, edited by J. A. Harvey and R. L. Macklin (USAEC CONF-710301, Knoxville, TN, 1971), p. 386.
[18] S. F. Mughabghab, M. Divadeenam, and N. E. Holden, *Neutron Cross Sections* (Academic Press, New York, 1981), Vol. 1.
[19] C. H. Johnson, C. Mahaux, and R. R. Winters, Phys. Rev. C **32**, 359 (1985).
[20] C. H. Johnson, R. F. Carlton, and R. R. Winters, Phys. Rev. C **39**, 415 (1989).
[21] P. P. Guss, R. C. Byrd, C. R. Howell, R. S. Pedroni, G. Tungate, and R. L. Walter, Phys. Rev. C **39**, 405 (1989).
[22] V. M. Timokhov, M. V. Bokhovko, A. G. Isakov, L. E. Kazakov, V. N. Kononov, G. N. Manturov, E. D. Poletaev, and V. G. Pronyaev, Sov. J. Nucl. Phys. **50**, 375 (1989).
[23] A. B. Popov and G. S. Samosvat, Radiat. Eff. **93**, 285 (1986).
[24] V. G. Soloviev, Ch. Stoyanov, and A. I. Vdoin, Joint Inst. Nucl. Res. Report **P4**-7499, 1973.
[25] M. S. Pandey, J. B. Garg, J. A. Harvey, and W. M. Good, Physics Division Annual Report ORNL-5025, 1975 (unpublished), p. 125.
[26] J. B. French and F. S. Chang, in *Statistical Properties of Nuclei*, edited by J. B. Garg (Plenum, New York, 1972), p. 421.